JACS
JOURNAL OF THE AMERICAN CHEMICAL SOCIETY
pubs.acs.org/JACS
Article

Spectral Stable Blue-Light-Emitting Diodes via Asymmetric Organic Diamine Based Dion–Jacobson Perovskites

Yuqiang Liu, Luis K. Ono, Guoqing Tong, Tongle Bu, Hui Zhang, Chenfeng Ding, Wei Zhang, and Yabing Qi*

Cite This: J. Am. Chem. Soc. 2021, 143, 19711–19718
Read Online
ACCESS | Metrics & More | Article Recommendations | Supporting Information

ABSTRACT: The spectral instability issue is a challenge in blue perovskite light-emitting diodes (PeLEDs). Dion–Jacobson (DJ) phase perovskites are promising alternatives to achieve high-quality blue PeLEDs. However, the current exploration of DJ phase perovskites is focused on symmetric divalent cations, and the corresponding efficiency of blue PeLEDs is still inferior to that of green and red ones. In this work, we report a new type of DJ phase $CsPb(Br/Cl)_3$ perovskite via introduction of an asymmetric molecular configuration as the organic spacer cation in perovskites. The primary and tertiary ammonium groups on the asymmetric cations bridge with the lead halide octahedra forming the DJ phase structures. Stable photoluminescence spectra were demonstrated in perovskite films owing to the suppressed halide segregation. Meanwhile, the radiative recombination efficiency of charges is improved significantly as a result of the confinement effects and passivation of charge traps. Finally, we achieved an external quantum efficiency of 2.65% in blue PeLEDs with stable spectra emission under applied bias voltages. To our best knowledge, this is the first report of asymmetric cations used in PeLEDs, which provides a facile solution to the halide segregation issue in PeLEDs.

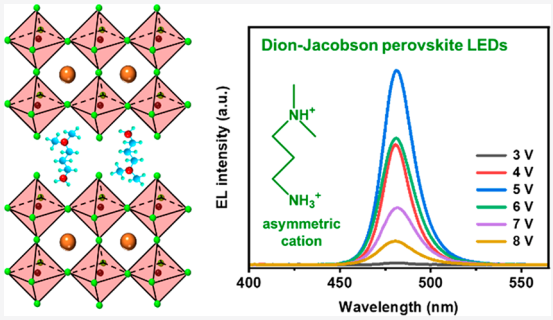

INTRODUCTION

Perovskite light-emitting diodes (PeLEDs) as promising light sources have progressed rapidly.[1−16] Currently, external quantum efficiencies (EQEs) over 20% have been demonstrated for green, red, and near-infrared PeLEDs.[17−20] However, the efficiency for blue PeLEDs is still substantially inferior as compared with other PeLEDs because of the halide segregation issue in the perovskite emitter films.[21,22] High-quality blue emitter layers are a prerequisite to the pursuit of high-efficiency blue PeLEDs. Generally, tailoring the three-dimensional (3D) bromide/chloride (Br/Cl) composition is a straightforward strategy for blue emitter perovskite layers. However, the electroluminescence (EL) instability poses a critical challenge in terms of Br/Cl phase segregation under applied bias voltage.[23,24] Wang et al. found that homogeneous distribution of Br/Cl halides in perovskite layers was favorable to overcome the phase segregation problem. As the homogeneity was increased by cationic surfactants, phase segregation was suppressed and therefore spectral stable blue PeLEDs were realized.[25] Gao et al. carried out a vapor-assisted crystallization technique to control the distribution of Br/Cl halides, and the homogeneous distribution led to the stable emission spectra and an encouraging EQE of 11% at 477 nm.[26] However, nonradiative recombination losses in 3D Br/Cl perovskites still markedly limit the performance of blue PeLEDs.

The exploration of quasi-2D perovskites, i.e., Ruddlesden–Popper (RP) and Dion–Jacobson (DJ) phases, provides a feasible strategy to eliminate the nonradiative recombination losses.[27,28] Because of the quantum/dielectric confinement effect from the low dimensional phase perovskites, the quantum efficiency was improved.[29,30] The incorporation of organic cations also passivated traps and reduced quenching losses effectively.[31,32] These effects synergistically increased the radiative recombination efficiency of the injected charges in perovskite emitter layers. For instance, through incorporation of phenylethylammonium bromide into $CsPb(Br/Cl)_3$ perovskites to prepare quasi-2D phases, nonradiative recombination losses were reduced effectively due to the confinement and passivation effects, yielding an EQE of 5.7% at the EL peak of 480 nm.[31] The chemical properties of organic cations and their corresponding 2D phase distribution are crucial factors for device performance.[33−35] DJ phase perovskites possessing closer and stronger bridges between lead halide octahedra than the RP phases are regarded as the potential schemes to achieve

Received: July 25, 2021
Published: November 18, 2021

https://doi.org/10.1021/jacs.1c07757
J. Am. Chem. Soc. 2021, 143, 19711–19718

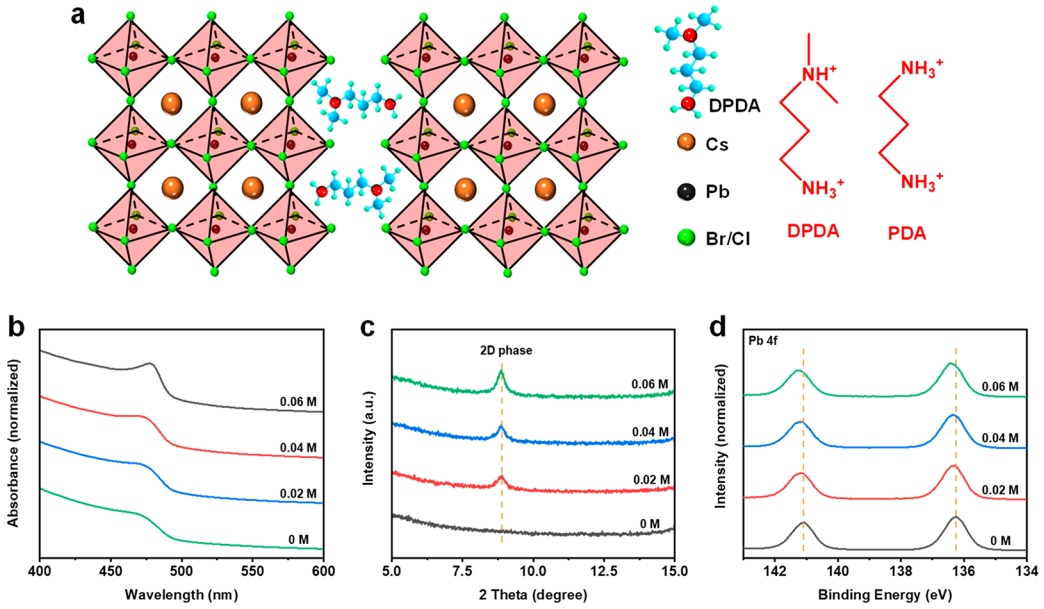

Figure 1. (a) Schematic illustration of the DJ phase perovskites and the chemical structure of the DPDA and PDA organic cations. (b) Absorption spectra, (c) XRD patterns, and (d) XPS spectra of the Pb $4f_{7/2}$ and Pb $4f_{5/2}$ core levels of the $CsPb(Br/Cl)_3$ perovskite films with different DPDA ratios: 0 M, 0.02 M, 0.04 M, and 0.06 M.

stable blue PeLEDs.[36−38] Incorporating divalent cations is the direct way to form DJ phase structures. There are two classes of divalent cations, i.e., symmetric and asymmetric cations. The exploration of organic cations in the DJ phase perovskites up to now is only concentrated on the symmetric class. Compared with symmetric cations with the same ammonium groups, the asymmetric ones consisting of two different ammonium groups may possess intriguing properties in perovskites and its concept has not been explored in PeLEDs yet.

Herein, an asymmetric divalent organic cation (*N*,*N*-dimethyl-1,3-propanediamine, DPDA) was introduced to prepare a new type of DJ phase perovskite for blue PeLEDs. DPDA cations were inserted into crystalline domains of $CsPb(Br/Cl)_3$ perovskite, forming 2D phase structures. The accompanying confinement effects enhanced the photoluminescence (PL) characteristics of perovskite emitter layers. Nonradiative recombination losses were eliminated effectively. Additionally, the phase segregation of Br/Cl was suppressed. The blue PeLEDs with DPDA-based perovskite emitters showed stable spectra emission under applied bias voltages. An EQE of 2.65% was obtained in blue PeLEDs at 481 nm. On the contrary, when the symmetric 1,3-diaminopropane (PDA) was used as organic cations, Br/Cl perovskites exhibited clear phase segregation, and the EL spectra shifted from blue to green.

RESULTS AND DISCUSSION

Dion−Jacobson Phase Perovskites. The nominal formula of DPDA-$CsPb(Br/Cl)_3$ perovskite was prepared by depositing a precursor solution containing $DPDABr_2$, CsBr, $PbBr_2$, and $PbCl_2$ in stoichiometric proportions (see Experimental Section in Supporting Information for details). Figure 1 illustrates the chemical structures of the DPDA and PDA organic cations. The DPDA cation displays an asymmetric structure consisting of a primary and a tertiary ammonium group. On the other hand, the PDA cation consists of two symmetric primary ammonium groups. The DPDA cations can be inserted into the perovskite crystals during the growth process. The ammonium group interacts with the lead halide octahedra by hydrogen bonding, and the adjacent octahedra slabs are bridged by the DPDA cations, forming the DJ phase perovskites, as shown in the schematic illustration in Figure 1. As a consequence, the absorption curves (Figure 1b) of the perovskite films shifted toward shorter wavelengths upon increasing DPDA ratios, because of the confinement effect of the low dimensional phases. X-ray diffraction (XRD) measurements were carried out to study the crystal structure of the DPDA-perovskites. According to the XRD patterns in Figure S1a, the peak width of the 3D diffraction peaks at 15.4° and 31.1° increased because of the incorporation of organic cations. In comparison with the 3D perovskite, the appearance of the new diffraction peak at 8.8° is associated with the incorporated DPDA cations (Figure 1c), which belongs to the one-layered DJ phase perovskites.[39] Meanwhile, as shown in Figure S1b, the diffraction peak at 31.1° shifted to a lower degree after incorporation of the DPDA cations, which could be attributed to the lattice expansion of perovskites. In other words, the DPDA was successfully inserted into the crystal structure of the perovskites. The grain size of the DPDA-perovskites is reduced compared with that of the 3D ones, as shown in scanning electron microscopy (SEM) images (Figure S2).

X-ray photoelectron spectroscopy (XPS) measurements were performed to study the interaction between the DPDA cations and perovskites. The XPS survey spectra of the different perovskite films are shown in Figure S3a. As shown in Figure 1d, the core levels of Pb $4f_{7/2}$ and Pb $4f_{5/2}$ shifted toward higher binding energies, and this shifting tendency was enhanced upon increasing the ratio of DPDA. This can be attributed to the changes in the chemical environment of Pb^{2+} in the PbI_6 octahedra, which hints the interaction between Pb^{2+} and DPDA. XPS curve fitting analyses in the N 1s and Pb $4f_{7/2}$ core level regions for the DPDA- and PDA-perovskite films have been performed to examine the interaction between DPDA and the $CsPb(Br/Cl)_3$ perovskite. Both XPS spectra in the N 1s region can be fitted with a single Gaussian−

https://doi.org/10.1021/jacs.1c07757
J. Am. Chem. Soc. 2021, 143, 19711−19718

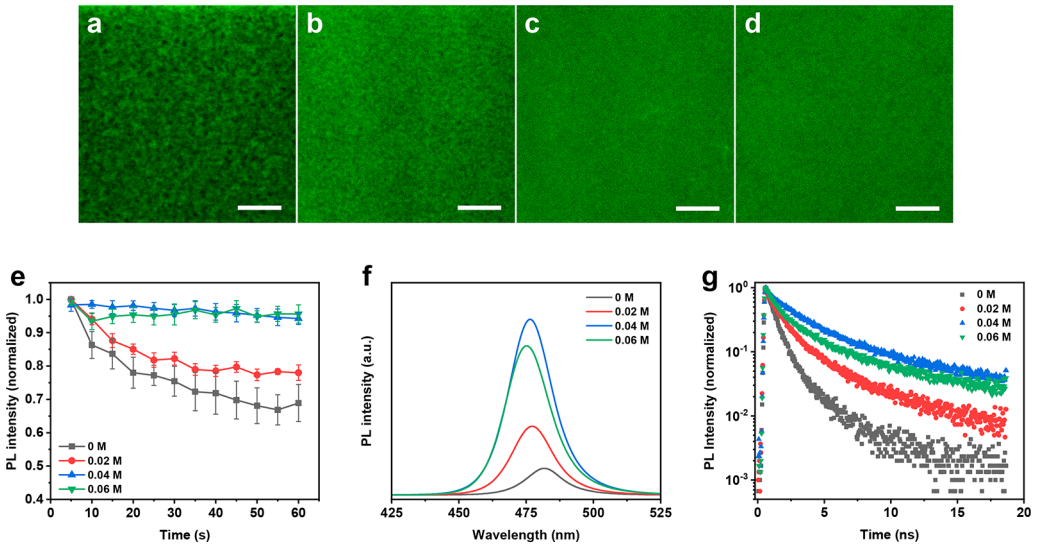

Figure 2. Confocal laser scanning fluorescence microscopy images of the perovskite films with different DPDA ratios: (a) 0 M, (b) 0.02 M, (c) 0.04 M, and (d) 0.06 M (all scale bars are 1 μm). (e) Fluctuation of time-dependent PL intensities of the perovskite films. (f) Steady-state PL spectra of the perovskite films. (g) Time-resolved PL spectra of the perovskite films.

Lorentzian shape line after the Shirley background fitting (Figure S3b). However, the DPDA-perovskite spectrum shows a slightly larger full-width at half-maximum (fwhm) when compared to the PDA-perovskite spectrum, which may infer the difference of the Pb^{2+} coordination between the primary amine and tertiary amine of DPDA. The fitted Pb $4f_{7/2}$ peaks in Figure S3c show similar fwhm values when comparing the pristine perovskite and the perovskites with PDA or DPDA molecules. Because (i) the binding energy separation of the N 1s signals from the primary amine and tertiary amine in DPDA is small and (ii) the different types of interactions between amine groups and the ions in the perovskite film (i.e., not only Pb^{2+}) coexist, it is challenging to thoroughly determine the distinction of Pb^{2+} coordination between the primary amine and tertiary amine using the XPS technique solely. Therefore, we would like to make a conservative view regarding this point, i.e., our XPS results hint that there likely exists a slight difference of the Pb^{2+} coordination between the primary amine and tertiary amine of DPDA, but a thorough understanding of this distinction requires further in-depth investigation.

Photoluminescence Characteristics. The confocal laser scanning fluorescence microscopy (CLSFM) technique was used to characterize the spatial uniformity of the perovskite phase by the PL distribution. As shown in Figure 2a, the control 3D perovskite film showed a nonuniform PL distribution with many dark regions. These dark regions were caused by the quenching of charges, i.e., a large number of charges lost through nonradiative recombination pathways in the 3D perovskite films. When 0.02 M DPDA was incorporated into perovskites, the PL distribution (Figure 2b) became more uniform compared with the film without DPDA. When the ratio of DPDA was increased to 0.04 M (Figure 2c) and 0.06 M (Figure 2d), a reasonably uniform PL distribution was obtained, in which the dark regions were eliminated dramatically. Meanwhile, the fluctuation of the time-dependent PL intensity was acquired by monitoring 10 individual points from the CLSFM mapping images. As shown in Figure 2e, a fast decay tendency of the PL intensity was detected for the 3D perovskite film. The decay tendency became slower as the DPDA ratio increased. Upon the incorporation of 0.04 M DPDA, the PL intensity of the perovskite film remained nearly constant as a function of time, which indicated that the nonradiative recombination pathway was eliminated effectively, and consequently the utilization of charges became effective.

Additionally, PL characterizations were performed to further check the recombination condition of perovskite films. According to the steady-state PL spectra in Figure 2f, the PL intensity increased significantly upon incorporation of DPDA, and the largest intensity was reached at the DPDA ratio of 0.04 M. The improved PL property is mainly ascribed to the following aspects: (i) low dimensional phase increased the radiative recombination efficiency of charges through confinement effects;[29,30] (ii) organic cations passivated the traps in perovskite, reducing the quenching losses.[31,32] Figure S4 is the optical photograph of the perovskite films without or with DPDA under ultraviolet radiation, and it demonstrated a stronger PL emission of the DPDA-perovskite films than that of the 3D ones. Meanwhile, both the average PL lifetime and photoluminescence quantum yield (PLQY) demonstrate the same tendency as the PL intensity. As shown in Figure 2g, the average PL lifetime (i.e., the period of time that it takes for the PL intensity to drop to 1/e of the initial intensity) of the 3D perovskite film was 1.3 ns. The average PL lifetimes were 1.7, 2.9, and 2.1 ns, corresponding to the DPDA ratio of 0.02, 0.04, and 0.06 M, respectively. The average PL lifetime of the perovskite-DPDA (0.04 M) film was more than twice that of the 3D one. As shown in Figure S5, the PLQY of the perovskite films increased from below 1% (0 M) to 10.7% after incorporation of 0.02 M DPDA. When the ratio reached 0.04 M, a PLQY value of 43.17% was realized. However, the PLQY value decreased once the DPDA incorporation ratio reached 0.06 M (PLQY of 24.6%).

Phase Segregation. Furthermore, the phase stability of perovskites with asymmetric DPDA and symmetric PDA was studied. Absorption spectra and steady-state PL spectra of perovskite films with DPDA (0.04 M) and PDA (0.04 M) were presented in Figure S6. PL measurements were carried out to examine the influences of DPDA and PDA on the dynamics of halide segregation in perovskite films. If Br/Cl halide

https://doi.org/10.1021/jacs.1c07757
J. Am. Chem. Soc. 2021, 143, 19711−19718

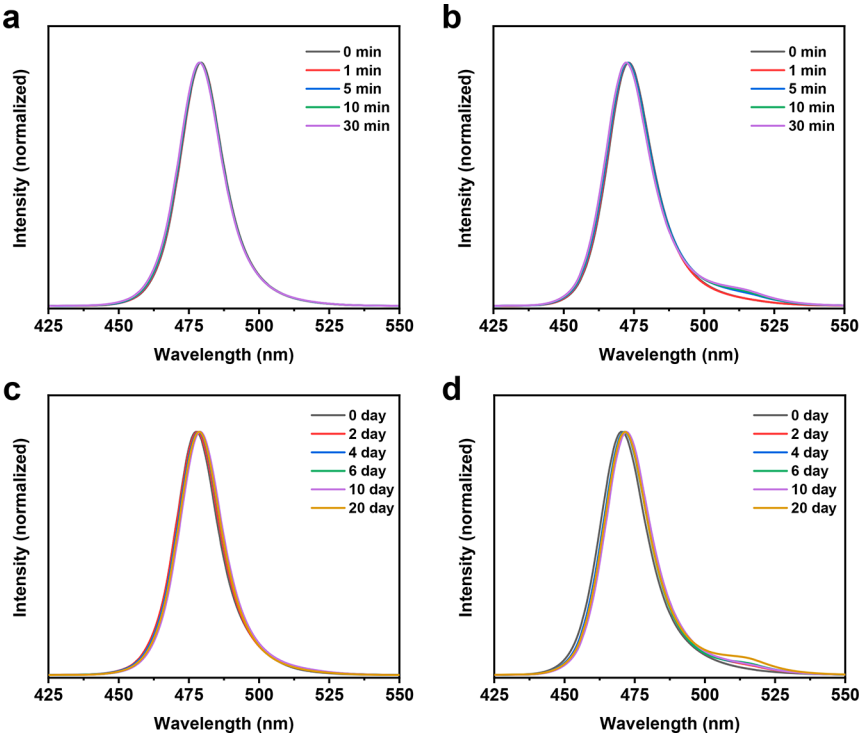

Figure 3. Steady-state PL spectra of the perovskite films with the DPDA or PDA cations: (a) DPDA- and (b) PDA-perovskite films under irradiation for 30 min; (c) DPDA- and (d) PDA-perovskite films stored in air for 20 days.

segregation takes place, new peaks would be observed during the continuous monitoring of the PL spectra.[40] Figure 3a displays the steady-state PL spectra of the DPDA-perovskite films within 30 min continuous irradiation. The PL peaks were stable without the appearance of additional peaks. On the contrary, new peaks appeared between 500 and 525 nm, when the PDA based perovskite films were exposed under continuous irradiation (Figure 3b and Figure S7a). The PL peaks between 500 and 525 nm came from the Br-rich phase perovskite. In other words, phase segregation existed in the PDA based perovskite films, forming Br-rich domains. Additionally, the property of phase stability in air was measured with a relative humidity of 15−20% and a temperature of 15−20 °C. Similarly, the DPDA-perovskite films demonstrated phase-stable property (Figure 3c), while the PDA-perovskite films could not keep phase stability and extra PL peaks (Figure 3d and Figure S7b) appeared after storing in air. Therefore, DPDA is more favorable to maintain the Br/Cl mixed perovskite phases than PDA.

Several reports have proposed the microscopic origins for the halide-segregation phenomena.[41−48] The dynamics of ion migration is complex and may involve a number of factors, such as trap state density, halide stoichiometry, light intensity, etc. Nevertheless, more and more researchers have reached the understanding that the excited charge carriers generated by photon absorption process[42,43] or applied bias (or charge injection)[44,45] are the major driving force for halide segregation. The unbalanced remaining charges, for example, hole accumulation on the halide site, were reported to induce the iodide ion to move from its original lattice toward the grain boundary induced by the local electric fields.[48] Therefore, efficient extraction of electrons and holes without accumulation from the perovskite is key to reducing ion migration. Recently, the A-cation site (size and dipole strength) has been reported to have a particular strong influence on the dynamics of halide segregation.[41,46,47] On the basis of theoretical calculations, it has been proposed that the activation energies for the halide movement follow the same trend as the dipole strength of A-cations.[41] The stronger dipole of A-cation can interact more effectively with the halide vacancy, leading to an effective screening/dispersion of the local charges (and local electric fields). This vacancy−dipole interaction results in a smaller distortion of the octahedra upon the halide vacancy formation, which increases the energy barrier for the halide migration.[41] On the basis of the aforementioned analyses, it is likely not a single factor, but the convoluted effects proposed above lead to the overall stability improvement. One of the plausible reasons that DPDA-perovskite maintained better phase stability is the dipole moment of the DPDA cations. Ion migration of Br/Cl halides is expected to be facilitated by the vacancies in perovskites. The asymmetric primary ammonium and tertiary ammonium groups on DPDA cations generate a dipole moment that can interact with these vacancies.

Ultraviolet photoemission spectroscopy (UPS) measurements were performed to study the dipole moment of the DPDA cations, as shown in Figure S8. The work function of the ITO film did not have a distinct change after depositing the PDA film. As a comparison, there was an improvement of ∼0.4 eV when PDA was replaced by the DPDA cations in perovskite films. Therefore, the dipole moment was associated with the DPDA cations. This vacancy−dipole interaction increases the activation energy of ion migration in perovskite films, eliminating the ion migration path effectively (Figure S9a).[41] As a consequence, the ion migration of Br/Cl is suppressed, and the stability of perovskite improves. To further verify this point, we measured the current−voltage characteristic curves of the perovskite films after poling at 1 V bias for 1 min.[49] A constant bias voltage was applied to the two parallel Au

https://doi.org/10.1021/jacs.1c07757
J. Am. Chem. Soc. 2021, 143, 19711−19718

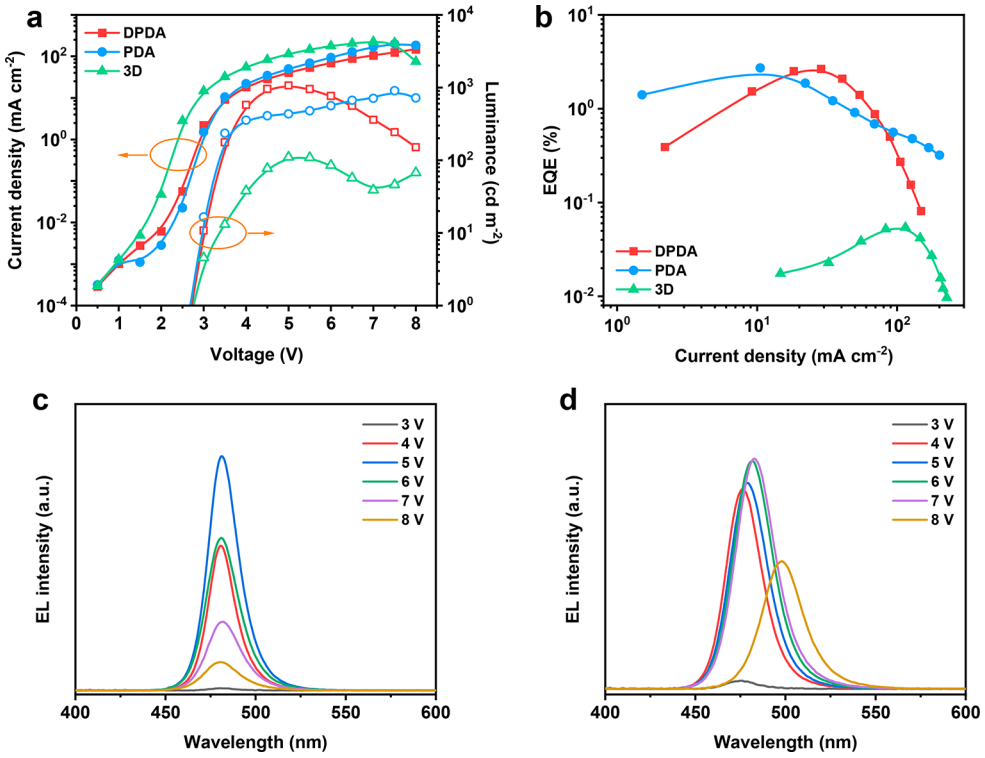

Figure 4. Optoelectronic characterization of the PeLED devices: (a) current density−luminance−voltage curves of the devices; (b) EQE−current density curves of the devices; (c) EL spectra of the devices with DPDA as the organic cations; (d) EL spectra of the device with PDA as the organic cations.

electrodes as shown in Figure S9b, and the electric field creates a driving force for ion migration in the perovskite films. When ion migration takes place in the perovskite films under the poling condition, the perovskite film will be changed to p/n types, and as a consequence, there is a built-in potential (voltage) in the perovskite films (more severe ion migration results in a higher voltage). According to the current−voltage characteristic curves in Figure S9c, when the current is 0, the corresponding voltage of the device based on the PDA-perovskite is larger than that of the device with the DPDA-perovskite. This result indicates that ion migration in the PDA-perovskite is more severe than that in the DPDA-perovskite.

Furthermore, we propose two other possible scenarios: (i) incorporation of asymmetric large cations results in stronger interactions between DPDA and the inorganic framework, which leads to perovskite grains with a more rigid structure;[50−52] (ii) organic cation-assisted high quality growth of perovskite grains with uniformly ordered cations surrounding the DJ perovskite grains and suppressed local strains (induced by grain boundaries) leads to suppression of ion migration.[52−54] The rigidity of the perovskite structure can be inferred from our XRD results (Figure S1b). When DPDA is incorporated, the perovskite peak at 31.1° shifted to a lower angle of ∼30.8° (0.04 M) corresponding to a total shift of ∼0.3° signifying the expansion in the lattice parameter. However, when PDA is incorporated in perovskite, the diffraction peak shift is much more significant: from ∼30.7° to ∼30.1°, corresponding to a total shift of ∼0.6°.[37] Because the shift of the diffraction peak to a lower angle signifies expansion in the lattice parameter of the perovskite crystal structure, the incorporation of asymmetric DPDA induces a lower lattice expansion, which leads to a higher structural rigidity in the perovskite framework in comparison to that employing the symmetric PDA molecules (justifying point i). Regarding point ii, we conducted the detailed XPS curve fitting analyses of the high-resolution N 1s and Pb $4f_{7/2}$ core-level regions to compare the DPDA- and DPA-perovskite films. Interestingly, the peak full width at half maximum increases is observed to broaden for the DPDA-perovskite film as compared with the PDA-perovskite film. This finding is consonant with the two different end groups in the asymmetric cation and the peak position shift (indicating the strength of the different interactions between the cations and perovskite), which suggests the stronger affinity between DPDA and the inorganic framework of perovskite.

Device Performance. Our PeLED devices used a structure of indium tin oxide (ITO)/modified-poly(3,4-ethylenedioxythiophene):poly(styrenesulfonate) (PEDOT:PSS)/perovskites/2,2′,2″-(1,3,5-benzenetriyl)tris(1-phenyl-1*H*-benzimidazole) (TPBi)/8-hydroxyquinolinolatolithium (Liq)/aluminum (Al). Figure 4a shows the current density−luminance−voltage curves of the devices. The highest luminance of the DPDA-perovskite device reached 1068 cd m^{-2}. However, it is hard to compare the highest luminance of the PDA-perovskite device because the electroluminescence (EL) spectra kept shifting during the characterization. The EQE−current density curves of the devices are displayed in Figure 4b. When DPDA-perovskite and PDA-perovskite were used as the emitter layers, the EQE reached 2.65% and 2.72%, respectively. Both are much higher than that of the 3D perovskite based devices, which has an EQE below 0.1%. Figure 4c shows the EL spectra of a device with the DPDA-perovskite emitter layer. The corresponding EL peaks were located at 481 nm and without obvious shift as the applied bias voltage was increased from 3 to 8 V. As a comparison, the EL spectra of the PDA-perovskite based device had a severe spectral shift from the blue to green

https://doi.org/10.1021/jacs.1c07757
J. Am. Chem. Soc. 2021, 143, 19711−19718

regions (Figure 4d). This spectral shift was caused by the phase segregation under the bias voltage. Hence, the perovskite film can maintain its phase structure under bias voltage, when DPDA was used as organic cations. The working half-life of the devices using the DPDA-perovskite as emitter layers is shown in Figure S10a. When the initial luminance was 100 cd/m^2, the half-life of the device was ∼2 min. Meanwhile, according to the half-life values, the EL spectra have no obvious shift during the operation period as shown in Figure S10b. In our study, via introduction of asymmetric DPDA cations, we have alleviated the phase segregation issue and increased the radiative recombination efficiency. On the other hand, the efficiency and lifetime of our DPDA-perovskite-based PeLED devices still have room to further improve. For example, to further increase the phase stability in Br/Cl mixed perovskite films, composition engineering will be a promising strategy to control halide migration and/or phase segregation to achieve highly efficient and stable PeLEDs.[36,55,56]

CONCLUSION

Phase stable blue PeLEDs are realized by incorporating asymmetric divalent organic cations. The DPDA cations lead to the formation of DJ phase perovskites. Radiative recombination efficiency is improved as a result of the confinement and passivation effects. Meanwhile, compared with the symmetric PDA cations, DPDA is more effective to suppress the phase segregation of Br/Cl halides. Finally, an EQE of 2.65% is realized in blue PeLEDs with stable EL emission.

ASSOCIATED CONTENT

Supporting Information

The Supporting Information is available free of charge at https://pubs.acs.org/doi/10.1021/jacs.1c07757.

Experimental section, XRD patterns, SEM images, XPS and UPS spectra, optical photographs, PLQY, absorption spectra, and steady-state PL spectra (PDF)

AUTHOR INFORMATION

Corresponding Author

Yabing Qi − *Energy Materials and Surface Sciences Unit (EMSSU), Okinawa Institute of Science and Technology Graduate University (OIST), Kunigami-gun, Okinawa 904-0495, Japan*; orcid.org/0000-0002-4876-8049; Email: Yabing.Qi@OIST.jp

Authors

Yuqiang Liu − *Energy Materials and Surface Sciences Unit (EMSSU), Okinawa Institute of Science and Technology Graduate University (OIST), Kunigami-gun, Okinawa 904-0495, Japan; College of Textiles & Clothing, Qingdao University, Qingdao 266071, China*; orcid.org/0000-0003-3494-6390

Luis K. Ono − *Energy Materials and Surface Sciences Unit (EMSSU), Okinawa Institute of Science and Technology Graduate University (OIST), Kunigami-gun, Okinawa 904-0495, Japan*; orcid.org/0000-0003-3176-1876

Guoqing Tong − *Energy Materials and Surface Sciences Unit (EMSSU), Okinawa Institute of Science and Technology Graduate University (OIST), Kunigami-gun, Okinawa 904-0495, Japan*

Tongle Bu − *Energy Materials and Surface Sciences Unit (EMSSU), Okinawa Institute of Science and Technology Graduate University (OIST), Kunigami-gun, Okinawa 904-0495, Japan*

Hui Zhang − *Energy Materials and Surface Sciences Unit (EMSSU), Okinawa Institute of Science and Technology Graduate University (OIST), Kunigami-gun, Okinawa 904-0495, Japan*

Chenfeng Ding − *Energy Materials and Surface Sciences Unit (EMSSU), Okinawa Institute of Science and Technology Graduate University (OIST), Kunigami-gun, Okinawa 904-0495, Japan*

Wei Zhang − *Energy Materials and Surface Sciences Unit (EMSSU), Okinawa Institute of Science and Technology Graduate University (OIST), Kunigami-gun, Okinawa 904-0495, Japan*

Complete contact information is available at: https://pubs.acs.org/10.1021/jacs.1c07757

Notes

The authors declare no competing financial interest.

ACKNOWLEDGMENTS

This work was supported by funding from the Energy Materials and Surface Sciences Unit of the Okinawa Institute of Science and Technology Graduate University, the OIST R&D Cluster Research Program, the OIST Proof of Concept (POC) Program, and JST A-STEP Grant JPMJTM20HS, Japan. We thank the OIST Micro/Nanofabrication Section and Imaging Section for the support.

REFERENCES

(1) Liu, X. K.; Xu, W.; Bai, S.; Jin, Y.; Wang, J.; Friend, R. H.; Gao, F. Metal Halide Perovskites for Light-Emitting Diodes. *Nat. Mater.* **2021**, *20*, 10−21.

(2) Quan, L. N.; Rand, B. P.; Friend, R. H.; Mhaisalkar, S. G.; Lee, T. W.; Sargent, E. H. Perovskites for Next-Generation Optical Sources. *Chem. Rev.* **2019**, *119*, 7444−7477.

(3) Tan, Z. K.; Moghaddam, R. S.; Lai, M. L.; Docampo, P.; Higler, R.; Deschler, F.; Price, M.; Sadhanala, A.; Pazos, L. M.; Credgington, D.; Hanusch, F.; Bein, T.; Snaith, H. J.; Friend, R. H. Bright Light-Emitting Diodes Based on Organometal Halide Perovskite. *Nat. Nanotechnol.* **2014**, *9*, 687−692.

(4) Cho, H.; Jeong, S. H.; Park, M. H.; Kim, Y. H.; Wolf, C.; Lee, C. L.; Heo, J. H.; Sadhanala, A.; Myoung, N.; Yoo, S.; Im, S. H.; Friend, R. H.; Lee, T. W. Overcoming the Electroluminescence Efficiency Limitations of Perovskite Light-Emitting Diodes. *Science* **2015**, *350*, 1222−1225.

(5) Song, J.; Li, J.; Li, X.; Xu, L.; Dong, Y.; Zeng, H. Quantum Dot Light-Emitting Diodes Based on Inorganic Perovskite Cesium Lead Halides ($CsPbX_3$). *Adv. Mater.* **2015**, *27*, 7162−7167.

(6) Wang, N.; Cheng, L.; Ge, R.; Zhang, S.; Miao, Y.; Zou, W.; Yi, C.; Sun, Y.; Cao, Y.; Yang, R.; Wei, Y.; Guo, Q.; Ke, Y.; Yu, M.; Jin, Y.; Liu, Y.; Ding, Q.; Di, D.; Yang, L.; Xing, G.; Tian, H.; Jin, C.; Gao, F.; Friend, R. H.; Wang, J.; Huang, W. Perovskite Light-Emitting Diodes Based on Solution-Processed Self-Organized Multiple Quantum Wells. *Nat. Photonics* **2016**, *10*, 699−704.

(7) Yao, J. S.; Ge, J.; Wang, K. H.; Zhang, G.; Zhu, B. S.; Chen, C.; Zhang, Q.; Luo, Y.; Yu, S. H.; Yao, H. B. Few-Nanometer-Sized α-$CsPbI_3$ Quantum Dots Enabled by Strontium Substitution and Iodide Passivation for Efficient Red-Light Emitting Diodes. *J. Am. Chem. Soc.* **2019**, *141*, 2069−2079.

(8) Kim, Y.-H.; Kim, S.; Kakekhani, A.; Park, J.; Park, J.; Lee, Y.-H.; Xu, H.; Nagane, S.; Wexler, R. B.; Kim, D.-H.; Jo, S. H.; Martínez-Sarti, L.; Tan, P.; Sadhanala, A.; Park, G.-S.; Kim, Y.-W.; Hu, B.;

Bolink, H. J.; Yoo, S.; Friend, R. H.; Rappe, A. M.; Lee, T.-W. Comprehensive Defect Suppression in Perovskite Nanocrystals for High-Efficiency Light-Emitting Diodes. *Nat. Photonics* **2021**, *15*, 148−155.
(9) Xiao, Z.; Kerner, R. A.; Zhao, L.; Tran, N. L.; Lee, K. M.; Koh, T.-W.; Scholes, G. D.; Rand, B. P. Efficient Perovskite Light-Emitting Diodes Featuring Nanometre-Sized Crystallites. *Nat. Photonics* **2017**, *11*, 108−115.
(10) Lai, W.-C.; Hsieh, W.-M.; Yang, S.-H.; Yang, J.-C.; Guo, T.-F.; Chen, P.; Lin, L.-J.; Hsu, H.-C. High-Performance Perovskite-Based Light-Emitting Diodes from the Conversion of Amorphous Spin-Coated Lead Bromide with Phenethylamine Doping. *ACS Omega* **2020**, *5*, 8697−8706.
(11) Singh, A.; Chiu, N.-C.; Boopathi, K. M.; Lu, Y.-J.; Mohapatra, A.; Li, G.; Chen, Y.-F.; Guo, T.-F.; Chu, C.-W. Lead-Free Antimony-Based Light-Emitting Diodes through the Vapor−Anion-Exchange Method. *ACS Appl. Mater. Interfaces* **2019**, *11*, 35088−35094.
(12) Zhao, L.; Yeh, Y. W.; Tran, N. L.; Wu, F.; Xiao, Z.; Kerner, R. A.; Lin, Y. L.; Scholes, G. D.; Yao, N.; Rand, B. P. In Situ Preparation of Metal Halide Perovskite Nanocrystal Thin Films for Improved Light-Emitting Devices. *ACS Nano* **2017**, *11*, 3957−3964.
(13) Protesescu, L.; Yakunin, S.; Bodnarchuk, M. I.; Krieg, F.; Caputo, R.; Hendon, C. H.; Yang, R. X.; Walsh, A.; Kovalenko, M. V. Nanocrystals of Cesium Lead Halide Perovskites ($CsPbX_3$, X = Cl, Br, and I): Novel Optoelectronic Materials Showing Bright Emission with Wide Color Gamut. *Nano Lett.* **2015**, *15*, 3692−3696.
(14) Shynkarenko, Y.; Bodnarchuk, M. I.; Bernasconi, C.; Berezovska, Y.; Verteletskyi, V.; Ochsenbein, S. T.; Kovalenko, M. V. Direct Synthesis of Quaternary Alkylammonium-Capped Perovskite Nanocrystals for Efficient Blue and Green Light-Emitting Diodes. *ACS Energy Lett.* **2019**, *4*, 2703−2711.
(15) Watanabe, S.; Tumen-Ulzii, G.; Cheng, T.; Matsushima, T.; Adachi, C. Origin and Suppression of External Quantum Efficiency Roll-Off in Quasi-Two-Dimensional Metal Halide Perovskite Light-Emitting Diodes. *J. Phys. Chem. C* **2020**, *124*, 27422−27428.
(16) Xie, C.; Zhao, X.; Ong, E. W. Y.; Tan, Z. K. Transparent Near-Infrared Perovskite Light-Emitting Diodes. *Nat. Commun.* **2020**, *11*, 4213.
(17) Chu, Z.; Ye, Q.; Zhao, Y.; Ma, F.; Yin, Z.; Zhang, X.; You, J. Perovskite Light-Emitting Diodes with External Quantum Efficiency Exceeding 22% Via Small-Molecule Passivation. *Adv. Mater.* **2021**, *33*, 2007169.
(18) Hassan, Y.; Park, J. H.; Crawford, M. L.; Sadhanala, A.; Lee, J.; Sadighian, J. C.; Mosconi, E.; Shivanna, R.; Radicchi, E.; Jeong, M.; Yang, C.; Choi, H.; Park, S. H.; Song, M. H.; De Angelis, F.; Wong, C. Y.; Friend, R. H.; Lee, B. R.; Snaith, H. J. Ligand-Engineered Bandgap Stability in Mixed-Halide Perovskite Leds. *Nature* **2021**, *591*, 72−77.
(19) Xu, W. D.; Hu, Q.; Bai, S.; Bao, C. X.; Miao, Y. F.; Yuan, Z. C.; Borzda, T.; Barker, A. J.; Tyukalova, E.; Hu, Z. J.; Kawecki, M.; Wang, H. Y.; Yan, Z. B.; Liu, X. J.; Shi, X. B.; Uvdal, K.; Fahlman, M.; Zhang, W. J.; Duchamp, M.; Liu, J. M.; Petrozza, A.; Wang, J. P.; Liu, L. M.; Huang, W.; Gao, F. Rational Molecular Passivation for High-Performance Perovskite Light-Emitting Diodes. *Nat. Photonics* **2019**, *13*, 418−424.
(20) Shen, Y.; Cheng, L. P.; Li, Y. Q.; Li, W.; Chen, J. D.; Lee, S. T.; Tang, J. X. High-Efficiency Perovskite Light-Emitting Diodes with Synergetic Outcoupling Enhancement. *Adv. Mater.* **2019**, *31*, 1901517.
(21) Park, M. H.; Kim, J. S.; Heo, J. M.; Ahn, S.; Jeong, S. H.; Lee, T. W. Boosting Efficiency in Polycrystalline Metal Halide Perovskite Light-Emitting Diodes. *ACS Energy Lett.* **2019**, *4*, 1134−1149.
(22) Ren, Z. W.; Wang, K.; Sun, X. W.; Choy, W. C. H. Strategies toward Efficient Blue Perovskite Light-Emitting Diodes. *Adv. Funct. Mater.* **2021**, *31*, 2100516.
(23) Ji, K.; Anaya, M.; Abfalterer, A.; Stranks, S. D. Halide Perovskite Light-Emitting Diode Technologies. *Adv. Opt. Mater.* **2021**, *9*, 2002128.
(24) Jiang, Y.; Wei, J.; Yuan, M. Energy-Funneling Process in Quasi-2D Perovskite Light-Emitting Diodes. *J. Phys. Chem. Lett.* **2021**, *12*, 2593−2606.
(25) Cheng, L.; Yi, C.; Tong, Y.; Zhu, L.; Kusch, G.; Wang, X.; Wang, X.; Jiang, T.; Zhang, H.; Zhang, J.; Xue, C.; Chen, H.; Xu, W.; Liu, D.; Oliver, R. A.; Friend, R. H.; Zhang, L.; Wang, N.; Huang, W.; Wang, J. Halide Homogenization for High-Performance Blue Perovskite Electroluminescence. *Research* **2020**, *2020*, 9017871.
(26) Karlsson, M.; Yi, Z.; Reichert, S.; Luo, X.; Lin, W.; Zhang, Z.; Bao, C.; Zhang, R.; Bai, S.; Zheng, G.; Teng, P.; Duan, L.; Lu, Y.; Zheng, K.; Pullerits, T.; Deibel, C.; Xu, W.; Friend, R.; Gao, F. Mixed Halide Perovskites for Spectrally Stable and High-Efficiency Blue Light-Emitting Diodes. *Nat. Commun.* **2021**, *12*, 361.
(27) Liang, A.; Wang, K.; Gao, Y.; Finkenauer, B. P.; Zhu, C.; Jin, L.; Huang, L.; Dou, L. Highly Efficient Halide Perovskite Light-Emitting Diodes via Molecular Passivation. *Angew. Chem., Int. Ed.* **2021**, *60*, 8337−8343.
(28) Jiang, Y.; Cui, M.; Li, S.; Sun, C.; Huang, Y.; Wei, J.; Zhang, L.; Lv, M.; Qin, C.; Liu, Y.; Yuan, M. Reducing the Impact of Auger Recombination in Quasi-2D Perovskite Light-Emitting Diodes. *Nat. Commun.* **2021**, *12*, 336.
(29) Yuan, M.; Quan, L. N.; Comin, R.; Walters, G.; Sabatini, R.; Voznyy, O.; Hoogland, S.; Zhao, Y.; Beauregard, E. M.; Kanjanaboos, P.; Lu, Z.; Kim, D. H.; Sargent, E. H. Perovskite Energy Funnels for Efficient Light-Emitting Diodes. *Nat. Nanotechnol.* **2016**, *11*, 872−877.
(30) Quan, L. N.; Zhao, Y.; Garcia de Arquer, F. P.; Sabatini, R.; Walters, G.; Voznyy, O.; Comin, R.; Li, Y.; Fan, J. Z.; Tan, H.; Pan, J.; Yuan, M.; Bakr, O. M.; Lu, Z.; Kim, D. H.; Sargent, E. H. Tailoring the Energy Landscape in Quasi-2D Halide Perovskites Enables Efficient Green-Light Emission. *Nano Lett.* **2017**, *17*, 3701−3709.
(31) Li, Z.; Chen, Z.; Yang, Y.; Xue, Q.; Yip, H. L.; Cao, Y. Modulation of Recombination Zone Position for Quasi-Two-Dimensional Blue Perovskite Light-Emitting Diodes with Efficiency Exceeding 5%. *Nat. Commun.* **2019**, *10*, 1027.
(32) Guo, Y.; Apergi, S.; Li, N.; Chen, M.; Yin, C.; Yuan, Z.; Gao, F.; Xie, F.; Brocks, G.; Tao, S.; Zhao, N. Phenylalkylammonium Passivation Enables Perovskite Light Emitting Diodes with Record High-Radiance Operational Lifetime: The Chain Length Matters. *Nat. Commun.* **2021**, *12*, 644.
(33) Qin, C.; Matsushima, T.; Potscavage, W. J.; Sandanayaka, A. S. D.; Leyden, M. R.; Bencheikh, F.; Goushi, K.; Mathevet, F.; Heinrich, B.; Yumoto, G.; Kanemitsu, Y.; Adachi, C. Triplet Management for Efficient Perovskite Light-Emitting Diodes. *Nat. Photonics* **2020**, *14*, 70−75.
(34) Liu, Y.; Cui, J. Y.; Du, K.; Tian, H.; He, Z. F.; Zhou, Q. H.; Yang, Z. L.; Deng, Y. Z.; Chen, D.; Zuo, X. B.; Ren, Y.; Wang, L.; Zhu, H. M.; Zhao, B. D.; Di, D. W.; Wang, J. P.; Friend, R. H.; Jin, Y. Z. Efficient Blue Light-Emitting Diodes Based on Quantum-Confined Bromide Perovskite Nanostructures. *Nat. Photonics* **2019**, *13*, 760−764.
(35) Liu, Y. Q.; Bu, T. L.; Ono, L. K.; Tong, G. Q.; Zhang, H.; Qi, Y. B. Phase Aggregation Suppression of Homogeneous Perovskites Processed in Ambient Condition toward Efficient Light-Emitting Diodes. *Adv. Funct. Mater.* **2021**, *31*, 2103399.
(36) Shang, Y.; Liao, Y.; Wei, Q.; Wang, Z.; Xiang, B.; Ke, Y.; Liu, W.; Ning, Z. Highly Stable Hybrid Perovskite Light-Emitting Diodes Based on Dion-Jacobson Structure. *Sci. Adv.* **2019**, *5*, eaaw8072.
(37) Liu, Y.; Ono, L. K.; Tong, G.; Zhang, H.; Qi, Y. B. Two-Dimensional Dion−Jacobson Structure Perovskites for Efficient Sky-Blue Light-Emitting Diodes. *ACS Energy Lett.* **2021**, *6*, 908−914.
(38) Mao, L.; Ke, W.; Pedesseau, L.; Wu, Y.; Katan, C.; Even, J.; Wasielewski, M. R.; Stoumpos, C. C.; Kanatzidis, M. G. Hybrid Dion-Jacobson 2D Lead Iodide Perovskites. *J. Am. Chem. Soc.* **2018**, *140*, 3775−3783.
(39) Zhao, W.; Dong, Q.; Zhang, J.; Wang, S.; Chen, M.; Zhao, C.; Hu, M.; Jin, S.; Padture, N. P.; Shi, Y. Asymmetric Alkyl Diamine Based Dion-Jacobson Low-Dimensional Perovskite Solar Cells with Efficiency Exceeding 15%. *J. Mater. Chem. A* **2020**, *8*, 9919−9926.

https://doi.org/10.1021/jacs.1c07757
J. Am. Chem. Soc. 2021, 143, 19711−19718

(40) Draguta, S.; Sharia, O.; Yoon, S. J.; Brennan, M. C.; Morozov, Y. V.; Manser, J. S.; Kamat, P. V.; Schneider, W. F.; Kuno, M. Rationalizing the Light-Induced Phase Separation of Mixed Halide Organic-Inorganic Perovskites. *Nat. Commun.* **2017**, *8*, 200.
(41) Pazoki, M.; Wolf, M. J.; Edvinsson, T.; Kullgren, J. Vacancy Dipole Interactions and the Correlation with Monovalent Cation Dependent Ion Movement in Lead Halide Perovskite Solar Cell Materials. *Nano Energy* **2017**, *38*, 537−543.
(42) Hoke, E. T.; Slotcavage, D. J.; Dohner, E. R.; Bowring, A. R.; Karunadasa, H. I.; McGehee, M. D. Reversible Photo-Induced Trap Formation in Mixed-Halide Hybrid Perovskites for Photovoltaics. *Chem. Sci.* **2015**, *6*, 613−617.
(43) Yoon, S. J.; Draguta, S.; Manser, J. S.; Sharia, O.; Schneider, W. F.; Kuno, M.; Kamat, P. V. Tracking Iodide and Bromide Ion Segregation in Mixed Halide Lead Perovskites during Photo-irradiation. *ACS Energy Lett.* **2016**, *1*, 290−296.
(44) Zhang, H.; Fu, X.; Tang, Y.; Wang, H.; Zhang, C.; Yu, W. W.; Wang, X.; Zhang, Y.; Xiao, M. Phase Segregation Due to Ion Migration in All-Inorganic Mixed-Halide Perovskite Nanocrystals. *Nat. Commun.* **2019**, *10*, 1088.
(45) Knight, A. J.; Borchert, J.; Oliver, R. D. J.; Patel, J. B.; Radaelli, P. G.; Snaith, H. J.; Johnston, M. B.; Herz, L. M. Halide Segregation in Mixed-Halide Perovskites: Influence of A-Site Cations. *ACS Energy Lett.* **2021**, *6*, 799−808.
(46) Ono, L. K.; Juarez-Perez, E. J.; Qi, Y. B. Progress on Novel Perovskite Materials and Solar cells with Mixed Cations and Halide Anions. *ACS Appl. Mater. Interfaces* **2017**, *9*, 30197−30246.
(47) DuBose, J. T.; Kamat, P. V. TiO_2-Assisted Halide Ion Segregation in Mixed Halide Perovskite Films. *J. Am. Chem. Soc.* **2020**, *142*, 5362−5370.
(48) Pazoki, M.; Jacobsson, T. J.; Kullgren, J.; Johansson, E.M. J.; Hagfeldt, A.; Boschloo, G.; Edvinsson, T. Photoinduced Stark Effects and Mechanism of Ion Displacement in Perovskite Solar Cell Materials. *ACS Nano* **2017**, *11*, 2823−2834.
(49) Cao, J.; Tao, S. X.; Bobbert, P. A.; Wong, C. P.; Zhao, N. Interstitial Occupancy by Extrinsic Alkali Cations in Perovskites and Its Impact on Ion Migration. *Adv. Mater.* **2018**, *30*, 1707350.
(50) Zhang, Y.; Liu, Y.; Xu, Z.; Yang, Z.; Liu, S. 2D Perovskite Single Crystals with Suppressed Ion Migration for High-Performance Planar-Type Photodetectors. *Small* **2020**, *16*, 2003145.
(51) Wei, D.; Ma, F.; Wang, R.; Dou, S.; Cui, P.; Huang, H.; Ji, J.; Jia, E.; Jia, X.; Sajid, S.; et al. Ion-Migration Inhibition by the Cation−π Interaction in Perovskite Materials for Efficient and Stable Perovskite Solar Cells. *Adv. Mater.* **2018**, *30*, 1707583.
(52) Ren, M.; Cao, S.; Zhao, J.; Zou, B.; Zeng, R. Advances and Challenges in Two-Dimensional Organic−Inorganic Hybrid Perovskites Toward High-Performance Light-Emitting Diodes. *Nano-Micro Lett.* **2021**, *13*, 163.
(53) Liu, Y.; Zheng, X.; Fang, Y.; Zhou, Y.; Ni, Z.; Xiao, X.; Chen, S.; Huang, J. Ligand Assisted Growth of Perovskite Single Crystals with Low Defect Density. *Nat. Commun.* **2021**, *12*, 1686.
(54) Liu, D.; Luo, D.; Iqbal, A. N.; Orr, K. W. P.; Doherty, T. A. S.; Lu, Z.-H.; Stranks, S. D.; Zhang, W. Strain analysis and engineering in halide perovskite photovoltaics. *Nat. Mater.* **2021**, *20*, 1337−1346.
(55) Shang, Y.; Li, G.; Liu, W.; Ning, Z. Quasi-2D Inorganic $CsPbBr_3$ Perovskite for Efficient and Stable Light-Emitting Diodes. *Adv. Funct. Mater.* **2018**, *28*, 1801193.
(56) Liu, Y.; Dong, Y.; Zhu, T.; Ma, D.; Proppe, A.; Chen, B.; Zheng, C.; Hou, Y.; Lee, S.; Sun, B.; Jung, E. H.; Yuan, F.; Wang, Y. K.; Sagar, L. K.; Hoogland, S.; Garcia de Arquer, F. P.; Choi, M. J.; Singh, K.; Kelley, S. O.; Voznyy, O.; Lu, Z. H.; Sargent, E. H. Bright and Stable Light-Emitting Diodes Based on Perovskite Quantum Dots in Perovskite Matrix. *J. Am. Chem. Soc.* **2021**, *143*, 15606−15615.

https://doi.org/10.1021/jacs.1c07757
J. Am. Chem. Soc. 2021, 143, 19711−19718